ECEN5134 Homework 5

Labib Sharrar

February 27, 2025

1 Problem (a): Comparing Hertzian and Wire Dipoles

First and foremost in FEKO, we create a Hertzian dipole using the *Electric Dipole* option. In a separate model we design a simple wire dipole. Since we are simulating at $100MHz$, the wavelength, (λ), is $3m$. Therefore, we design the wire dipole to have a length of $\frac{\lambda}{50}$, which equates to $0.06m$. To make the wire dipole resemble the properties of a Hertzian dipole, we need its radius r to be small, such that $r << \lambda$. We choose $r = 0.001m$.

After the design phase is complete, the gain patterns (only E-plane is plotted, and H-plane would be circular since dipole is omnidirectional), directivity, and half-power beam widths (HPBW) of the Hertzian and wire dipoles are compared. It should be noted that since both dipoles are loss-less by default, the gain is equivalent to directivity.

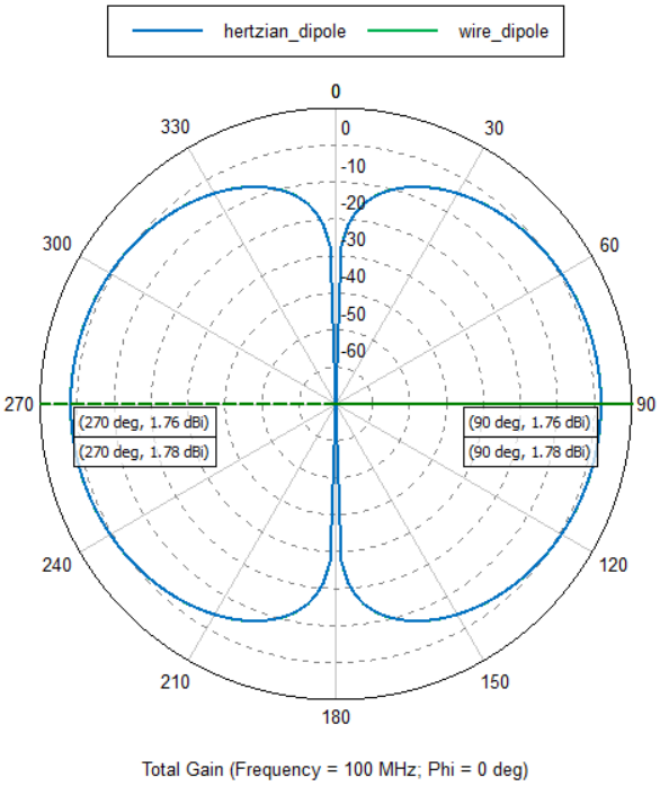

Figure 1: E-plane gain comparison of the Hertzian and the wire dipoles at $\phi = 0°$ cut.

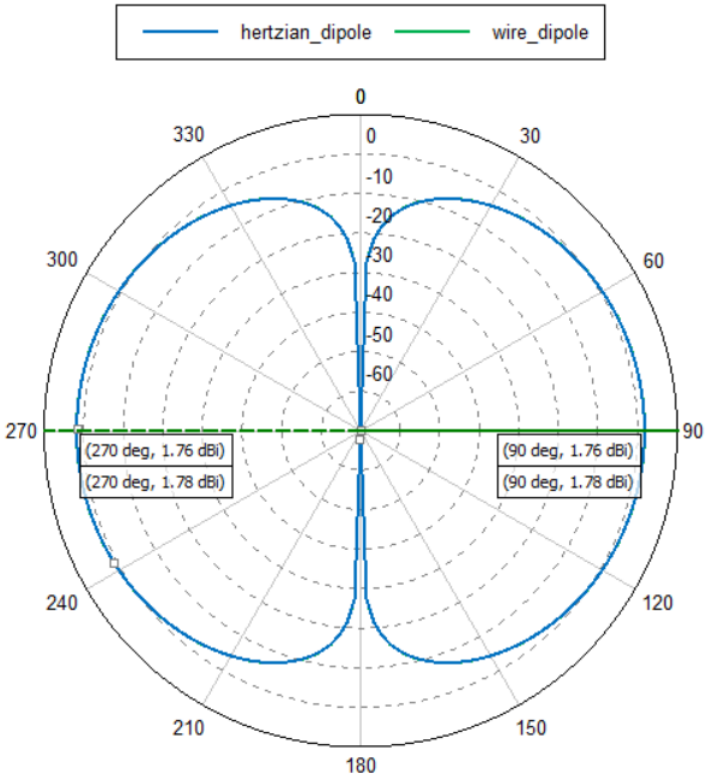

Figure 2: Comparing directivity of the Hertzian and the wire dipoles at $\phi = 0°$ cut.

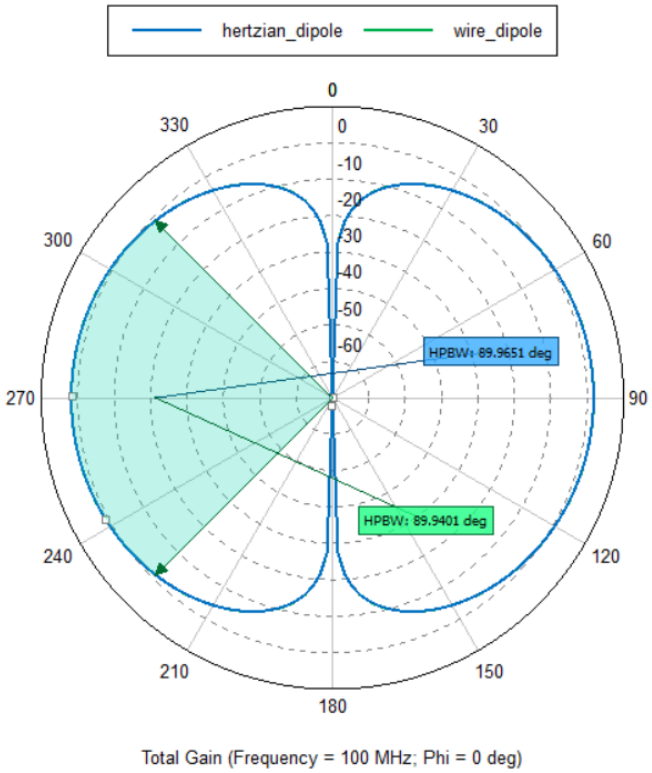

Figure 3: Comparing HPBW of the Hertzian and the wire dipoles.

Based on the above plots, we can tabulate the results as follows.

Antenna Type	Gain (dBi)	Directivity (dBi)	HPBW(°)
Hertzian Dipole	1.76	1.76	89.97
Wire Dipole	1.78	1.78	89.94

Table 1: Comparing results for Hertzian and wire dipoles.

From the table, we can see that the properties of the two dipoles are very close and almost indistinguishable. This makes sense, since a small dipole and a Hertzian dipole should ideally have the same gain and directivity.

2 Problem (b): Near-field Computations

Based on the properties of the dipole we can compute the radius of the radian sphere using $\frac{\lambda}{2\pi}$, which equates to approximately $0.48m$. Therefore, around the dipole, we form two concentric circles of radius $3mm$ and $6m$. The overall setup is shown in the following figure.

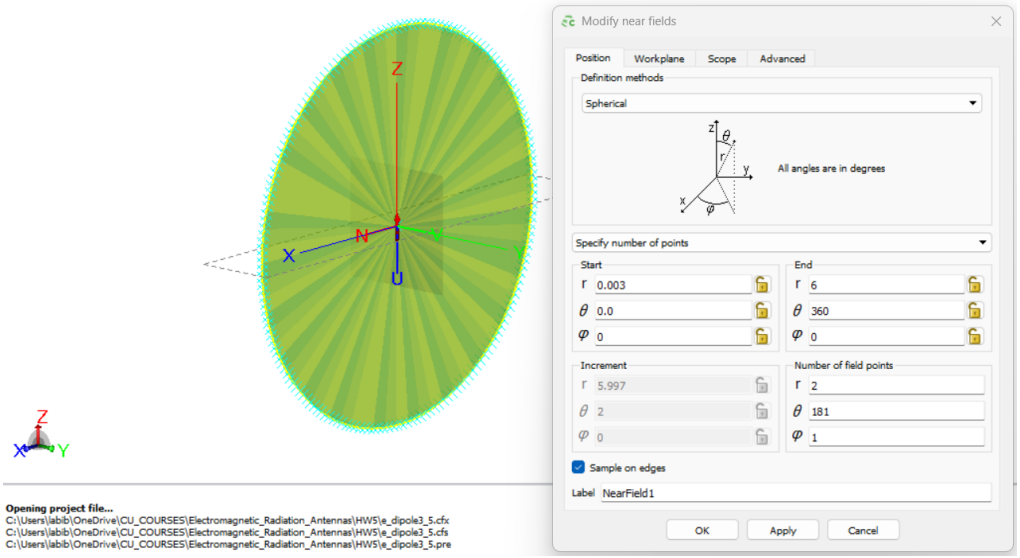

Figure 4: Concentric circles around the dipole.

For each circle, we plot E_r, E_θ and H_ϕ. To validate the plots, we use the equations relating to near-field and far-field equations, which are taken from the lecture slides. For simpler references later on, let us refer to these equations as **radian sphere equations**.

$$E_r = \eta \frac{I_0 l cos(\theta)}{2\pi r^2} \left[1 + \frac{1}{jkr}\right] e^{-jkr} \tag{1}$$

$$E_\theta = j\eta \frac{kI_0 l sin(\theta)}{4\pi r} \left[1 + \frac{1}{jkr} - \frac{1}{(kr)^2}\right] e^{-jkr} \tag{2}$$

$$E_\phi = 0 \tag{3}$$

$$H_r = H_\theta = 0 \tag{4}$$

$$H_\phi = j \frac{kI_0 l}{4\pi r} sin(\theta) \left[1 + \frac{1}{jkr}\right] e^{-jkr} \tag{5}$$

In the above equations, the notations l, r and I_0 represent the length of the dipole, radius of the radian sphere and the peak current across the dipole respectively. The circle with radius (r) $3mm$ is in the near-field. The plots of E and H planes for $r = 3mm$ is shown as follows. It should be noted that in these plots we have real and imaginary parts. In these plots, which are made on the Cartesian plane, have positive and negative directions. **However, we should look purely at the magnitude of the**

real and imaginary parts, rather than the direction. This should be done to understand whether the real or imaginary part dominates.

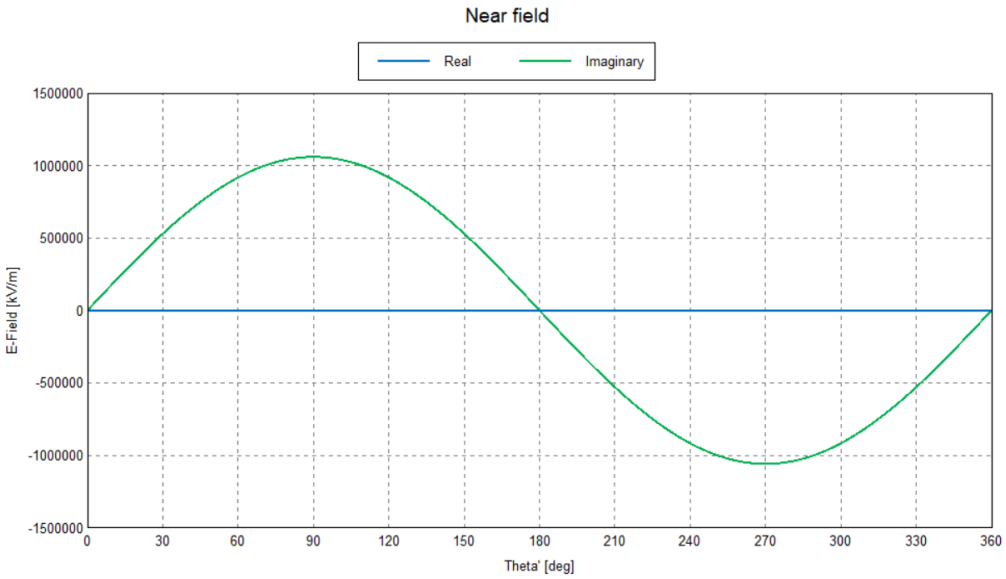

Figure 5: Plot of E_r for $r = 3mm$.

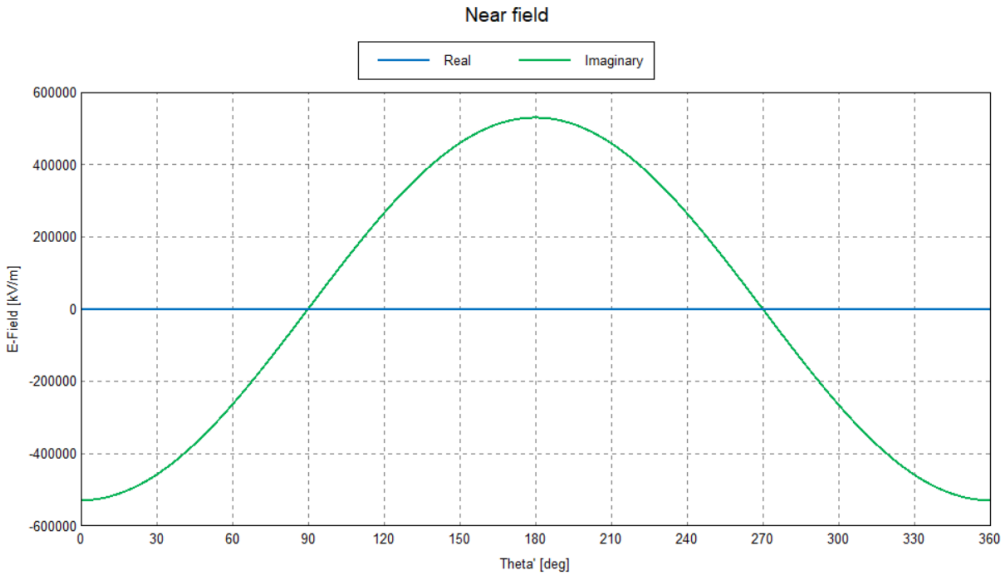

Figure 6: Plot of E_θ for $r = 3mm$.

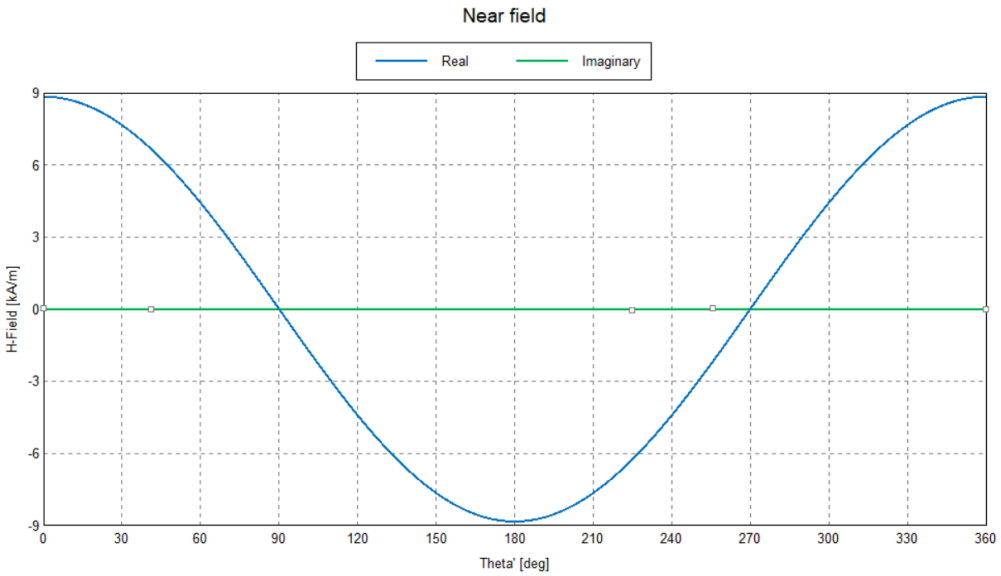

Figure 7: Plot of H_ϕ for $r = 3mm$.

From the above plots we can see that for E_r and E_θ the imaginary part dominates. As for H_ϕ, the real part is dominating. These observations align with the radian sphere equations and this can be validated through analysis. Given that $r = 3mm$, we get $kr << 1$. As a result, the radian sphere equations can be reduced to:

$$E_r = -j\eta \frac{I_0 l e^{-jkr}}{2\pi r^3} cos(\theta) \tag{6}$$

$$E_\theta = -j\eta \frac{I_0 l e^{-jkr}}{4\pi k r^3} sin(\theta) \tag{7}$$

$$E_\phi = 0 \tag{8}$$

$$H_r = H_\theta = 0 \tag{9}$$

$$H_\phi = \frac{I_0 l e^{-jkr}}{4\pi r^2} sin(\theta) \tag{10}$$

In the above equation, we see that E_r and E_θ are imaginary, while H_ϕ is real valued. This aligns with above plots, proving that the results for the near-field are as expected.

In regards to far-field, $kr >> 1$, where $r = 6m$, the plots of E_r, E_θ and H_ϕ are shown below.

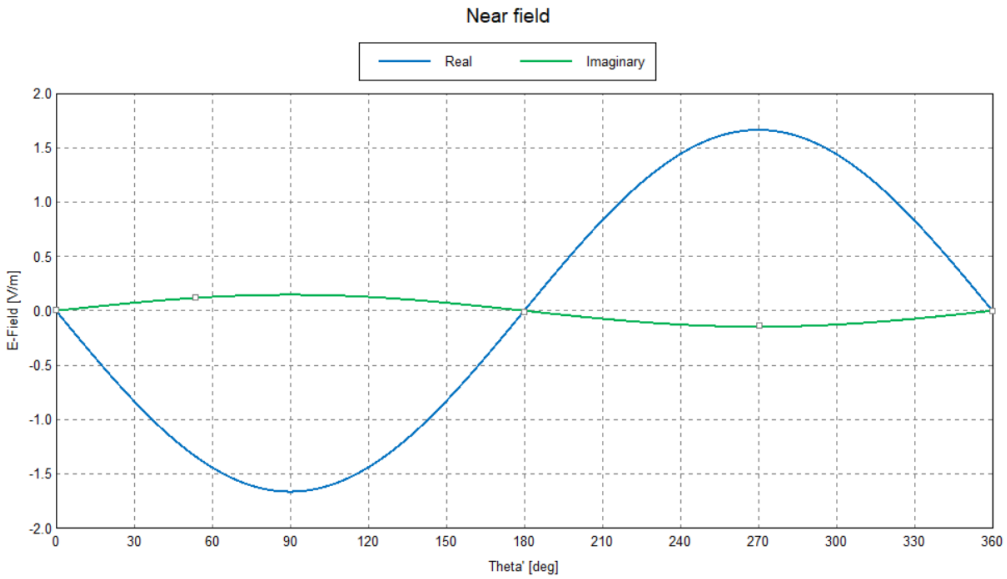

Figure 8: Plot of E_r for $r = 6m$.

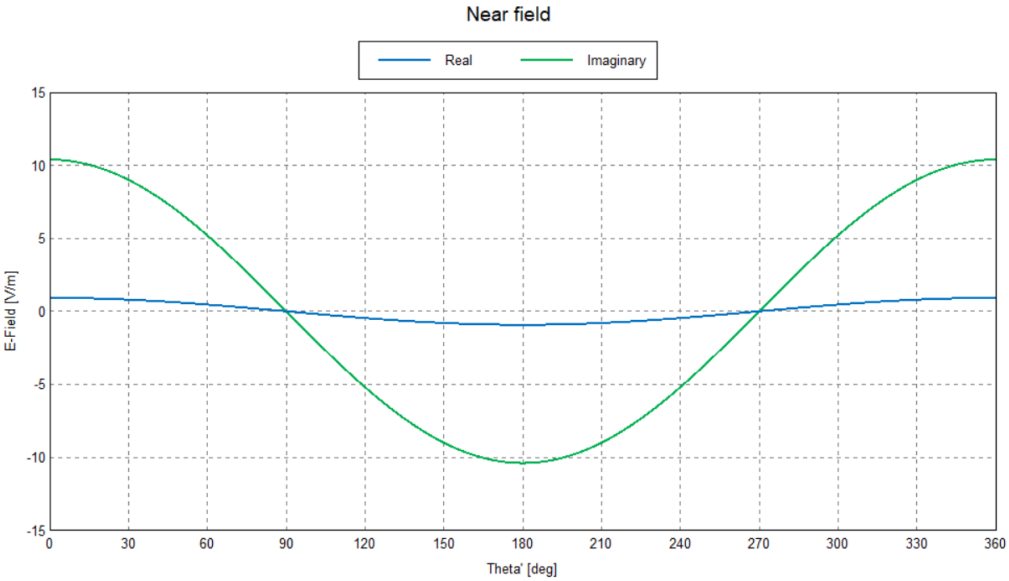

Figure 9: Plot of E_θ for $r = 6m$.

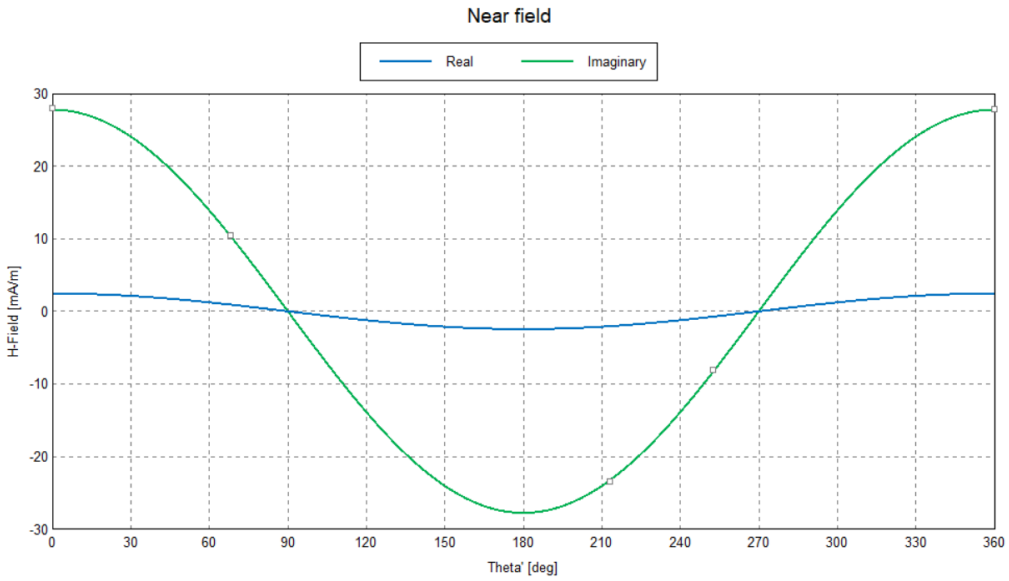

Figure 10: Plot of H_ϕ for $r = 6m$.

From the plots in Figures 8 to 10, we can see that for E_θ and H_ϕ the imaginary part dominates, while for E_r the real part dominates. These results align with the overall radian sphere equations, which can be reduced to as shown below. These reductions occur as a result of $kr >> 1$.

$$E_r = \eta \frac{I_0 l e^{-jkr}}{2\pi r^2} cos(\theta) \tag{11}$$

$$E_\theta = j\eta \frac{k I_0 l e^{-jkr}}{4\pi r} sin(\theta) \tag{12}$$

$$E_\phi = 0 \tag{13}$$

$$H_r = H_\theta = 0 \tag{14}$$

$$H_\phi = j \frac{k I_0 l e^{-jkr}}{4\pi r} sin(\theta) \tag{15}$$

In the equations presented above, it is evident that in the far-field region, E_r is real-valued, whereas E_θ and H_ϕ are imaginary. This observation confirms that even at a distance of $r = 6m$, the simulation results are consistent with the theoretical predictions outlined by the radian sphere equations.

Overall, the analysis in this section conclusively demonstrates that the simulation outcomes for both near-field and far-field scenarios accurately adhere to the corresponding mathematical formulations.

Note: For this question, the Hermitian dipole was used instead of the small dipole. A reason for this, is that for the small dipole in the near field the real part kept dominating the imaginary part when it should have been the other way around. FEKO seemed to give warning that for the near-fiel, the real part is computed incorrectly. I went to the office hours on Tuesday and everyone had the same problem. I have consulted Aadesh and he asked me to use the Hermitian dipole instead since in this case my simulation results are matching the mathematical expectations.

3 Problem (c): Dipole Current Distribution

By meshing, the wire dipole is divided into segments. The model is simulated to obtain the current distribution across different parts of the dipole. Based on the plot below, we can see that from one end of the dipole, the current magnitude rises until it reaches the maximum level at the middle of the dipole (marked by the $30th$ index). As the current departs from the middle, the current magnitude declines (with a symmetric negative gradient) until it reaches the end. Thus, we have a triangular current distribution across the dipole, with the maximum point in the middle.

As the frequency is altered, the triangular current distribution remains. However, the overall magnitude of the current increases with the frequency. Furthermore, as the frequency increases, the current distribution across the dipole changes with a steeper gradient.

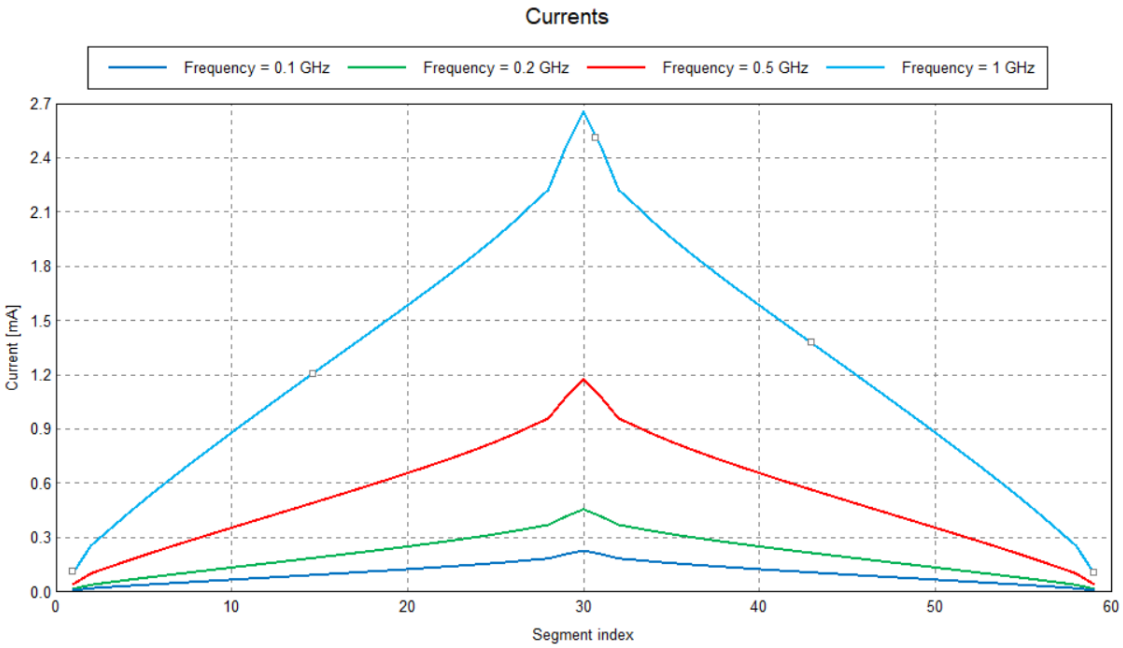

Figure 11: Distribution of current across the wire dipole for different frequencies.

The peak current, I_0, for different frequencies are recorded in the following table. As the frequency rises, the maximum peak current increases. At $1GHz$, the overall current is the highest, and a reason for this is that the around $1GHz$, the dipole approaches its resonance frequency.

Frequency (GHz)	I_0 **(mA)**
0.1	0.2266
0.2	0.4552
0.5	1.173
1	2.656

Table 2: Maximum current across frequencies.

As for the gain patterns at the different frequencies, we can refer to the following polar plot.

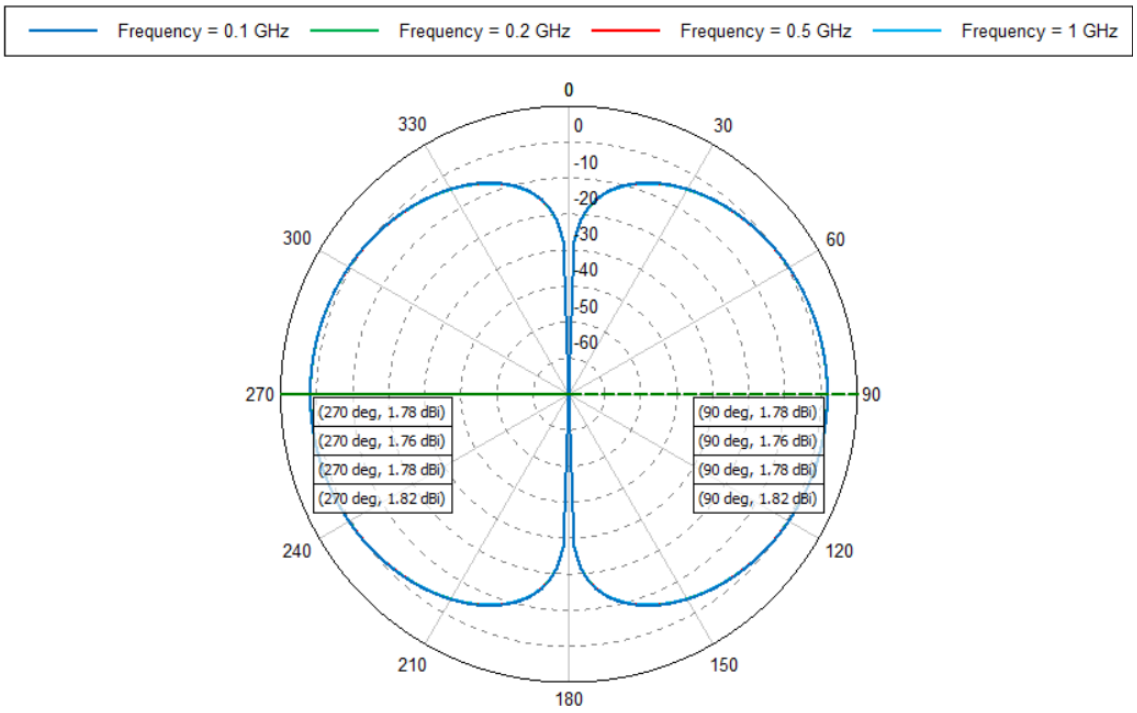

Figure 12: Gain pattern for different frequencies at $\phi = 0°$ cut.

The maximum gain for the different frequencies are recorded in the following table.

Frequency (GHz)	**Gain (dBi)**
0.1	1.78
0.2	1.76
0.5	1.78
1	1.82

Table 3: Maximum gain across different frequencies.

Overall, from $0.1GHz$ to $0.5GHz$, the maximum gain remains more or less the same. At $1GHz$, since the current is maximum, the gain rises to $1.82dBi$.

4 Problem (d): Dipole with Loading Plates

To the dipole from the previous section, capacitive loading plates of radius $0.04m$ are added. An image of the setup in FEKO is shown below.

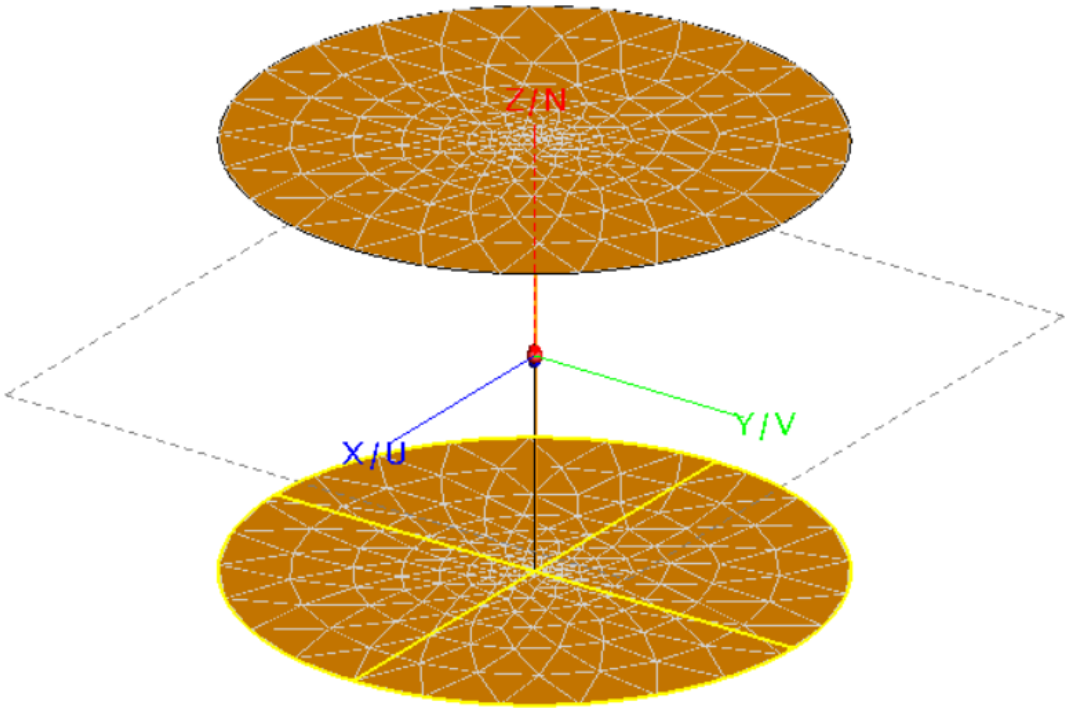

Figure 13: Dipole with capacitive loading plates.

After setting up the model, we plot the current distribution for different frequencies. For ease of visualization (in magnitude scale the difference between the current at $0.5GHz$ and other frequencies look too wide), and just for this case, the current distribution is plotted in logarithmic scale.

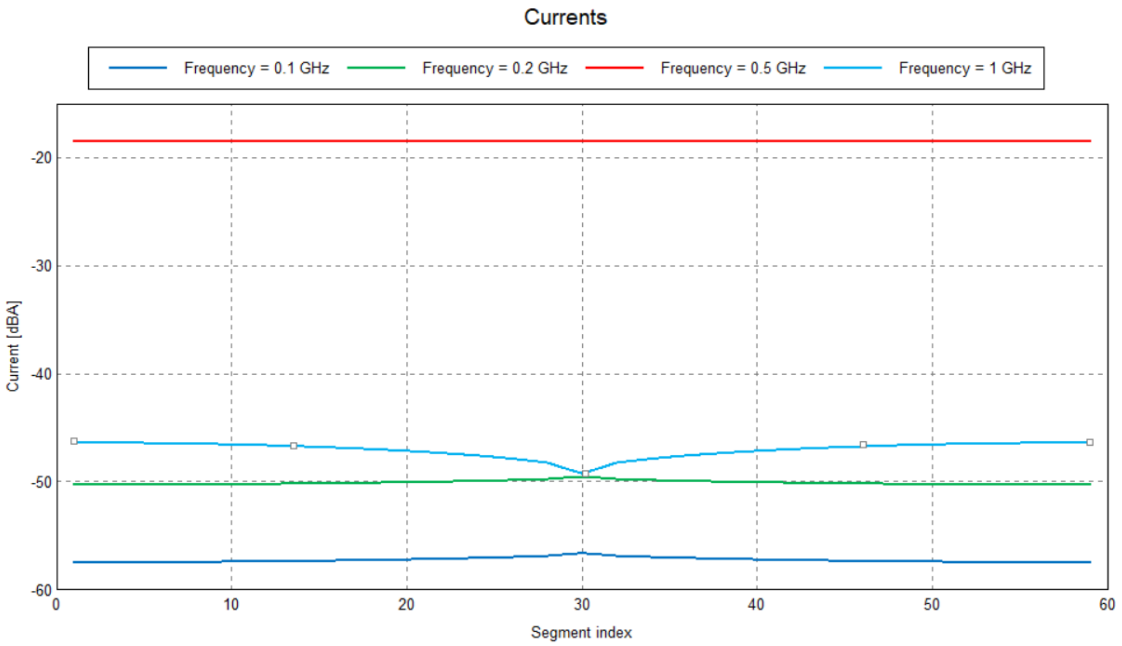

Figure 14: Current distribution across different frequencies (plotted in dB scale for better visualization).

In actuality, the current distribution across this model for different frequencies has a triangular formation (like in the previous subsection). However, this is barely noticeable. The current distributions look almost like straight horizontal lines. This is reasonable, since adding capacitive loads make the current distribution more uniform across the different parts of the dipole.

Compared to the previous subsection, another difference we notice is the the current at $0.5GHz$ is the highest. This happens because the overall model achieves resonant frequency around $0.5GHz$ as we can see from the plot below.

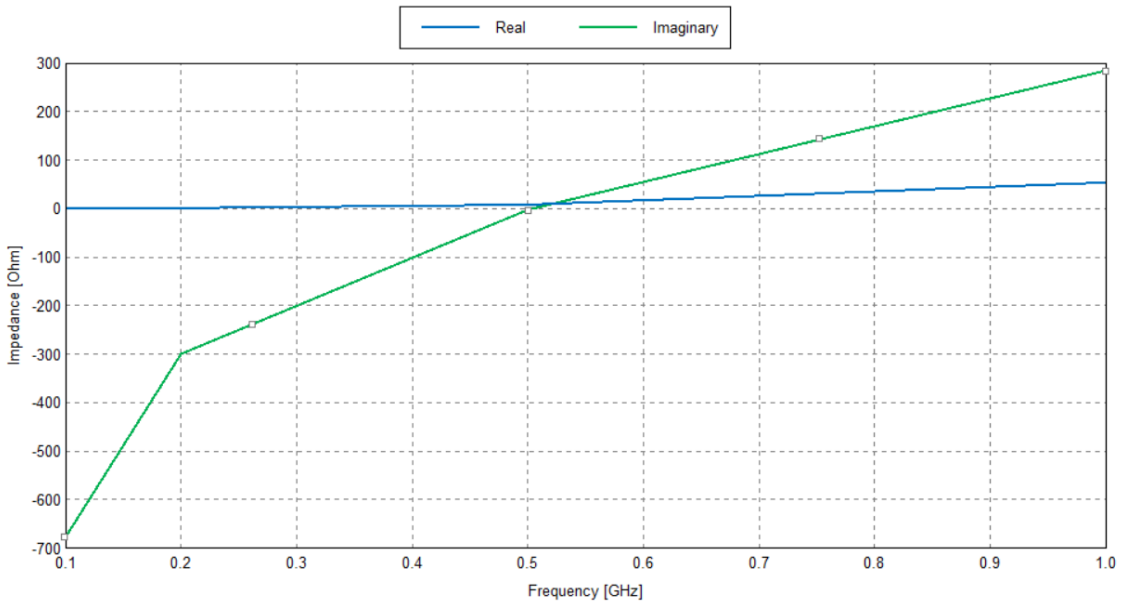

Figure 15: Impedance with the loading cells.

Furthermore, at $1GHz$, the current distribution seems to have a minimum value at the center of the dipole. The current distribution shows a minimum at the center because the antenna behaves like two half-wave dipoles end-to-end. This results in a node (point of minimum current) at the center of

the antenna, where the two half-wavelengths meet, and antinodes (points of maximum current) at the ends and the midpoint of each half-wavelength segment. This pattern is characteristic of a full-wave dipole, where a complete wavelength fits along the antenna's length, leading to a phase shift of 180° across the midpoint, thereby causing destructive interference and resulting in minimal current at that point.

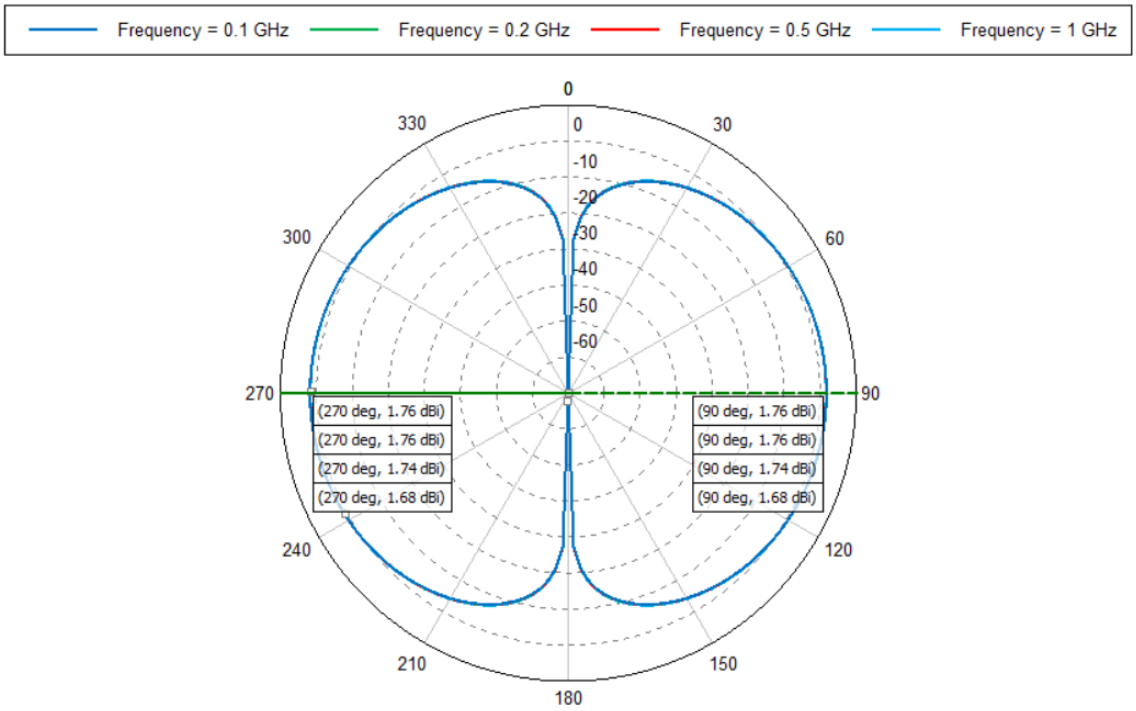

Figure 16: Gain pattern for different frequencies at $\phi = 0°$ cut.

Frequency (GHz)	**Gain (dBi)**
0.1	1.76
0.2	1.76
0.5	1.74
1	1.68

Table 4: Maximum current across different frequencies with the loading cells.

From the above table we can see that at $1GHz$, the maximum gain is the lowest. Since the current is minimum at the center of the dipole at $1GHz$, the peak gain at this frequency is the lowest.